Article

DFT Prediction of Factors Affecting the Structural Characteristics, the Transition Temperature and the Electronic Density of Some New Conjugated Polymers

Quoc-Trung Vu [1,*], **Thi-Thuy-Duong Tran [1]**, **Thuy-Chinh Nguyen [2]**, **Thien Vuong Nguyen [2]**, **Hien Nguyen [1]**, **Pham Van Vinh [3]**, **Dung Nguyen-Trong [3]**, **Nguyen Dinh Duc [4,5]** and **Phuong Nguyen-Tri [6,7,*]**

[1] Faculty of Chemistry, Hanoi National University of Education, 136 Xuan Thuy, Cau Giay, Hanoi 180000, Vietnam; tttthuyduong93@gmail.com (T.-T.-D.T.); hiennguyendhsphn@gmail.com (H.N.)

[2] Institute for Tropical Technology, Vietnam Academy of Science and Technology, 18, Hoang Quoc Viet, Cau Giay, Hanoi 122300, Vietnam; thuychinhhn@gmail.com (T.-C.N.); vuongvast@gmail.com (T.V.N.)

[3] Faculty of Physics, Hanoi National University of Education, 136 Xuan Thuy, Cau Giay, Hanoi 100000, Vietnam; vinhpv@hnue.edu.vn (P.V.V.); dungntsphn@hnue.edu.vn (D.N.-T.)

[4] Faculty of Environmental and Food Engineering, Nguyen Tat Thanh University, 300A Nguyen Tat Thanh, District 4, Ho Chi Minh City 755414, Vietnam; nguyensyduc@gmail.com

[5] Department of Environmental Energy Engineering, Kyonggi University, Suwon 16227, Korea

[6] Institute of Research and Development, Duy Tan University, Da Nang 550000, Vietnam

[7] Department of Chemistry, Biochemistry and Physics, University of Quebec in Trois-Rivieres (UQTR), Trois-Rivieres, QC G8Z 4M3, Canada

* Correspondence: trungvq@hnue.edu.vn (Q.-T.V.); phuong.nguyen-tri@uqtr.ca (P.N.-T.)

check for updates

Abstract: Conjugated polymers are promising materials for various cutting-edge technologies, especially for organic conducting materials and in the energy field. In this work, we have synthesized a new conjugated polymer and investigated the effect of distance between bond layers, side-chain functional groups (H, Br, OH, OCH_3 and OC_2H_5) on structural characteristics, phase transition temperature (T), and electrical structure of $C_{13}H_8OS$ using Density Functional Theory (DFT). The structural characteristics were determined by the shape, network constant (a, b and c), bond length (C–C, C–H, C–O, C–S, C–Br and O–H), phase transition temperatures, and the total energy (E_{tot}) on a base cell. Our finding shows that the increase of layer thickness (h) of $C_{13}H_8OS$–H has a negligible effect on the transition temperature, while the energy bandgap (E_g) increases from 1.646 eV to 1.675 eV. The calculation of bond length with different side chain groups was carried out for which $C_{13}H_8OS$–H has C–H = 1.09 Å; $C_{13}H_8OS$–Br has C–Br = 1.93 Å; $C_{13}H_8OS$–OH has C–O = 1.36 Å, O–H = 0.78 Å; $C_{13}H_8OS$–OCH_3 has C–O = 1.44 Å, O–H =1.10 Å; $C_{13}H_8OS$–OC_2H_5 has C–O = 1.45 Å, C–C = 1.51Å, C–H = 1.10 Å. The transition temperature (T) for $C_{13}H_8OS$–H was 500 K < T < 562 K; $C_{13}H_8OS$–Br was 442 K < T < 512 K; $C_{13}H_8OS$–OH was 487 K < T < 543 K; $C_{13}H_8OS$–OCH_3 was 492 K < T < 558 K; and $C_{13}H_8OS$–OC_2H_5 was 492 K < T < 572 K. The energy bandgap (E_g) of Br is of E_g = 1.621 eV, the doping of side chain groups H, OH, OCH_3, and OC_2H_5, leads to an increase of E_g from 1.621 eV to 1.646, 1.697, 1.920, and 2.04 eV, respectively.

Keywords: conjugated polymers; density functional theory; bond length; transition temperatures

1. Introduction

In recent years, conjugated polymers have been being widely studied and used in science and technology as well as in semiconductor devices [1,2], sensors [3–9], batteries [10,11], super-capacitors [10,12], electromagnetic shielding materials [13,14], and corrosion-resistant materials [15–20]. The properties of these materials may be greatly affected by doping/introduction of various substituents groups due to a modification of the electronic density of the molecules. Polypyrrole (PPr) is one of the most popular electrically-conducting polymers [21]. Some experimental studies on the electrical density showed that a pyrrole cation contains four pyrrole units. Bredas et al. using the Hartree Fock method and the STO-3G-based kit suggested that pyrrole did not have Na dopant [22]. With the theoretical method, the use of quantum calculations by the ab initio methods at a simple level cannot accurately describe the electronic structure of polypyrrole.

Recently, only a few studies have used the Density Functional Theory (DFT) method to study the electronic structure [23–27]. The electronic structure results show that the influence of the forbidden bandwidth on the impurity concentration and E_g can be adjusted by doping with different atoms [28–31]. Thereby, if the polymer is doped with an appropriate concentration, it can switch from being a semiconductor to a metal or back to an insulating material [32–35]. This has attracted particular attention from researchers to determine the transition between conductors and insulators such as transistors, light-emitting diodes, and solar cells [36]. For this purpose, it is necessary to control the bandgap doping. Some recent studies have shown promising results based on calculations through the original principles [37–44].

Rittmeyer et.al successfully used DFT to study the derived $C_{13}H_8OS$ in which an H atom was replaced by functional groups, viz. CH_3, NH_2, NO_2, and Cl. The results showed a significant influence of the substitutional elements on the bandgap. The absorption spectrum showed that the bandgap and optical properties are closely related to the shape of the thiophene molecule [45,46]. Most recently, our research group empirically studied $C_{13}H_8OS–X$ monomers (X = H, Br, OH, OCH_3 and OC_2H_5) that were synthesized from thiophene-3-carbaldehyde [47]. Their structures were confirmed by FTIR, ^{1}H-NMR, and ^{13}C-NMR spectroscopy. The crystal and molecular structures of $C_{13}H_8OS–H$, $C_{13}H_8OS–Br$, $C_{13}H_8OS–OH$, $C_{13}H_8OS–OCH_3$, and $C_{13}H_8OS–OC_2H_5$ were characterized by X-ray diffraction. We showed that the chemical polymerization of monomers $C_{13}H_8OS–FeCl_3$ in chloroform had been performed, as recently reported [48–51]. The obtained results show that the bonding lengths between atoms 1 and 2 are: C–C with Br (1.33 Å), OH (1.33 Å), OCH_3 (1.33 Å), and OC_2H_5 (1.32 Å); as well as C–O with Br (1.22 Å), OH (1.23 Å), OCH_3 (1.23 Å), and OC_2H_5 (1.22 Å) [47]. However, the effect of doping structure on the structural shape, the transition temperature and the electronic structure of the monomer $C_{13}H_8OS–X$ (X are: H, Br, OH, OCH_3, OC_2H_5) is still unknown. The main goal of this work is to answer to this fundamental and important question by/using DFT method, which have been successfully used for various materials.

2. Method of Calculation

Scheme 1 presents the synthetic procedure of the poly ($C_{13}H_8OS–X$) where X are H, Br, OH, OCH_3 and OC_2H_5. To study the structural characteristics, transition temperatures and electronic structure of poly[3-(3-phenyl prop-1-ene-3-one-1-yl)thiophene], DFT [52–55] with the DMol3 module [54] of the copyrighted Material Studio software, a commercial software package installed at the Center for a Computational Science of the Hanoi University of Education (Hanoi, Vietnam) was used. This is a modeling and simulation with the GGA package [56] for which the parameters of the PW91 exchange-correlation function [57,58] and the K-point grid sampling of the diagram Monkhorst-Pack [59] were set into a tridimensional cell unit with a defined dimensions a, b, and c as follows: poly($C_{13}H_8OS–H$) (a = 20 Å, b = 13 Å, c = 6 Å), $C_{13}H_8OS–Br$ (a = 26 Å, b = 13 Å, c = 6 Å), poly($C_{13}H_8OS–OH$) (a = 26 Å, b = 13 Å, c = 6 Å), $C_{13}H_8OS–OCH_3$ (a = 29 Å, b = 13 Å, c = 6 Å) and $C_{13}H_8OS–OC_2H_5$ (a = 32 Å, b = 13 Å, c = 6 Å). The electrons interact with each other through the Density Function Semi-core Pseudo-Potential [60] and thus the electrons are considered in a homogeneous

state. The energy was set at 1×10^{-6} eV, the displacement during the geometry optimization is at level 1×10^{-5} Ha/integer, and 5×10^{-3} Å.
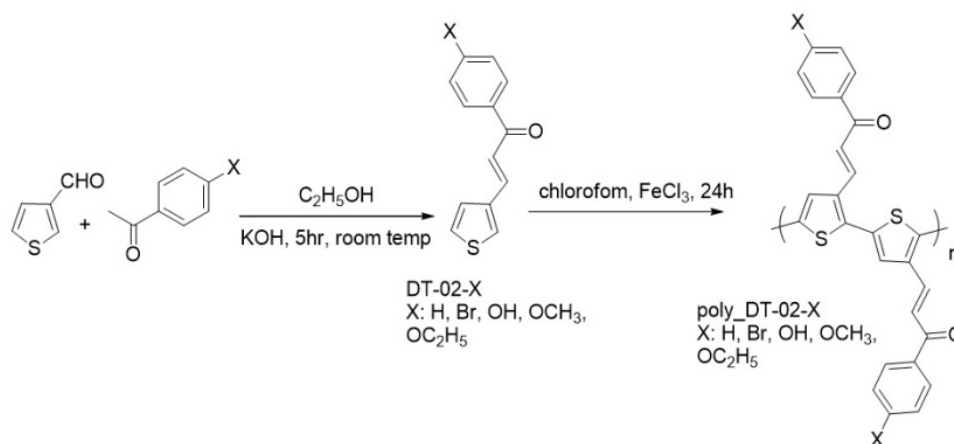

Scheme 1. The synthetic procedure of poly($C_{13}H_8OS$–X), X is H, Br, OH, CH_3, C_2H_5.

The DFT methods [61,62] have been established based on following approaches: Schrodinger model [63,64], Hartree-Fock model [65,66], Thomas-Fermi model [63], Hohenberg theorem [63,67,68] and traditional Kohn-Sham Theory [63,67,69]. To verify the accuracy of results, other methods such as Linear-Muffin-Tin-Orbital (LMTO) [70] method, Korringa-Kohn-Rostocker (KKR) methods [71] and General gradient approximation method (GGA) [72] has been reported.

## 3. Results and Discussion

3.1. Effect of Distance between Layers

Initially, all $C_{13}H_8OS$–X, X = H, Br, OH, CH_3 and C_2H_5 samples were run optimally so that all samples were returned to equilibrium. The results obtained for poly($C_{13}H_8OS$–H) are shown in Figure 1.
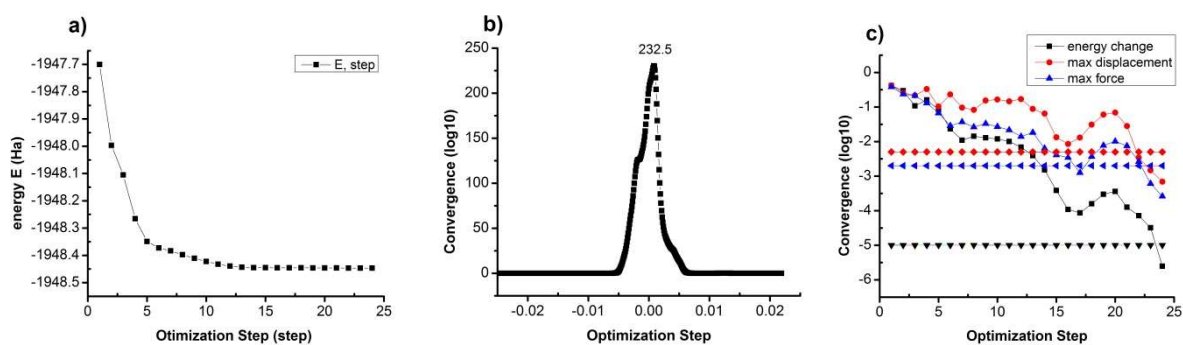
Figure 1. System energy (**a**), electronic density (**b**), electronic state (**c**) of poly($C_{13}H_8OS$–H) with a different number of steps.

Figure 1 shows that with $C_{13}H_8OS$–H, when increasing the number of steps, the total energy of the system (E_{tot}) will decrease from $E_{tot} = -1947.7$ eV to $E_{tot} = -1948.4$ eV (Figure 1a). There is a change in electronic density. The maximum value at the equilibrium position is of 232.5 eV (Figure 1b) and the electronic state decreases (Figure 1c) with the number of steps. The results show also that if the number of steps increases, the material will change from the initial state to the equilibrium state. The structural and electronic characteristics of materials in equilibrium state as a function of step number is conducted with a thickness of layers (h), h = 6 Å. The obtained results are presented in Figure 2 and summarized in Table 1.

Figure 2 shows that the shape of $C_{13}H_8OS–X$ after stable running NVE has $C_{13}H_8OS–H$ poly-structures and the atoms C, H, S, O are arranged tightly in a stable triclinic 3D structure. At the same time, the distance between atoms with the change of values by cell size: a = 24 Å, b = 13 Å, c = 6 Å, $\alpha = \beta = \gamma = 90^o$ the distance between atoms with the first round C–C varies from 1.39 Å to 1.41 Å, C–H: 1.09 Å. The interval between round one and round two: C–C: varies from 1.36 Å to 1.50 Å, C–O: 1.25 Å, C–H: 1.09 Å. The obtained results are completely consistent with the structural determination [47] for which C–C = 1.33 Å, C–O =1.23 Å. The second round: C–C = 1.36–1.42 Å, C–S = 1.72 Å, C–H: 1.09 Å, C–H: 1.09 Å. The bond angle of round one: C–C–C: changes from 120.17° to 120.8°, HCC: 120.02°, C–C–C connection interval: 119.21°, C–C–O: 119.7° to 121.08°, C–C–H: 119.26° to 121.16°. The bond angle of round two: C–C–C changes from 120.17° to 120.80° and H–C–C: 120.18°, C–C–C: 93.22°, C–S–C: 114.17°, S–C–C: 108.82°, C–C–H: 122.61°, S–C–H: 119.25° (Figure 2a) and electronic density at different levels of the conduction band (Table 1, Figure 2d). The transition temperature of poly($C_{13}H_8OS–H$) materials is found to be 504 K < T < 558 K (Figure 2b). Here T_c = 504 K is called the crystalline temperature (the temperature of transferring materials from liquid state to crystalline state), melting point (T_m = 558 K) is the phase transition temperature (the temperature of transferring materials from the crystalline state to the liquid state), the width forbidden region is of E_g = 1.646 eV (Figure 2c), the electronic density in equilibrium has the maximum value of 235 eV (Figure 2d). In particular, the electronic structure features are shown in Figure 2c with a strip structure in the left table and the density of electrons in the right table poly($C_{13}H_8OS–H$) is a semiconductor material with a bandgap of E_g = 1.646 eV. These results are consistent with the electronic densities of the states on the right of Table 1.
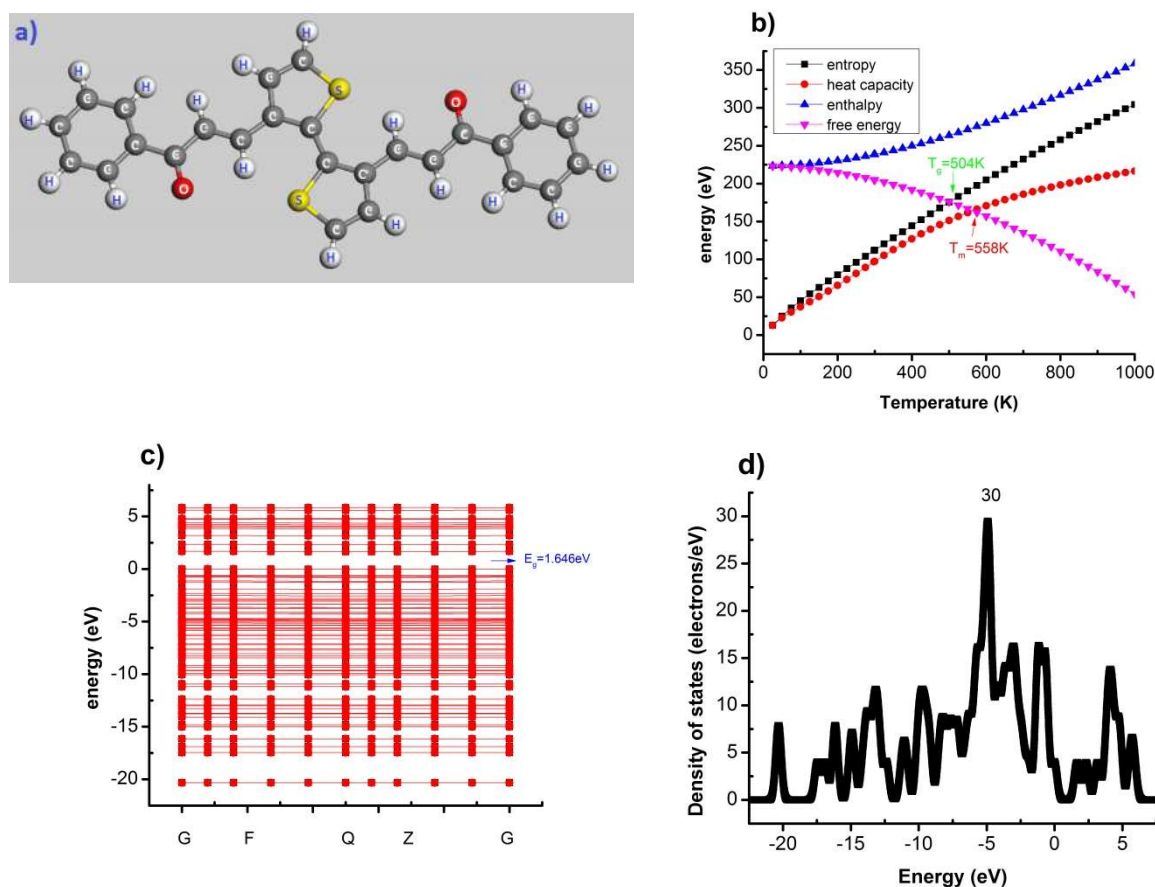
Figure 2. The quantities characteristic of the structure, and electronic structure of poly($C_{13}H_8OS–H$) materials such as Shape (**a**), phase transition temperature zone (**b**), electronic structure (**c**), and the density of states (**d**).

Table 1. The electron density for materials poly($C_{13}H_8OS–H$) at different energies in the valence bands.

Poly($C_{13}H_8OS–H$)	−20	−15	−10	−5	−2.5	0	2.5	5
Electron density	2.334	6.625	9.423	29.462	8.925	4.011	2.629	4.151

The results show that at the E = −5 eV the electron density is 29.462%, which shows that in the valence band, the electronic density reaches the maximum value, which proves that poly($C_{13}H_8OS–H$) is a semiconductor material. To study the effect of thickness between poly atomic layers, the results are shown in Table 2.

Table 2. Electron density for materials poly($C_{13}H_8OS–H$) with energies and thickness of layers different in the valence.

d(Å)	6	9	12	15
T(K)	504 < T < 558	504 < T < 564	504 < T < 564	504 < T < 564
E_g(eV)	1.646	1.675	1.675	1.675

Table 2 shows that, with h = 6 Å, the temperature range of poly($C_{13}H_8OS–H$) materials is 504 K < T < 558 K, where T_c = 504 K, T_m = 558 K, and the energy band gap E_g is of 1.646 eV. When the thickness (h) of the atomic layer increases from h = 6 Å to h = 9 Å, 12 Å and 15 Å, the temperature range of poly($C_{13}H_8OS–H$) has a negligible change between 504 and 564 K and E_g increases from E_g = 1.646 eV to E_g = 1.675 eV. The bandgap has a constant value when h > 9 Å (Table 2) which indicates that the smaller the atomic distance, the smaller the bandgap.

The increasing distance of the atomic layer leads to E_g increases and reaches to a maximum value at h = 9 Å. For more details, the total density of the states of the poly $C_{13}H_8OS–H$ material with increasing thickness of the layers at the density of the states at different energies in the valence band and the conduction band is conducted. The obtained results are shown in Figure 3.

A maximum value of electronic density of poly($C_{13}H_8OS–H$) material as a function of atomic layer distance is observed at creating energy band of E = −5 eV, assigned to the electronic density as follows: with h = 6 Å is 29.462%, h = 9 Å, 12 Å, and 15 Å with the electronic density in the valence band has constant value of 29.463%. It turns out that the highest electron density level leads to the least flexible conductivity because the electrons are closely linked to the network node. Increasing the thickness of the atomic layers of poly($C_{13}H_8OS–H$) leads to an increase of the density of electrons in the valence band, after that this effect is less pronounced with a slight increase from 4.011% to 4.018%. Electron density not significantly changed in the conduction band at h = 6 Å, in which electron density in the conduction band of poly($C_{13}H_8OS–H$) increases at E = 2.5 eV (Figure 3), leading to a decrease of the mobility of electrons in the valence band. This shows an important effect of bond layers, on the structural characteristics, the transition temperature, and electronic properties of poly($C_{13}H_8OS–H$).
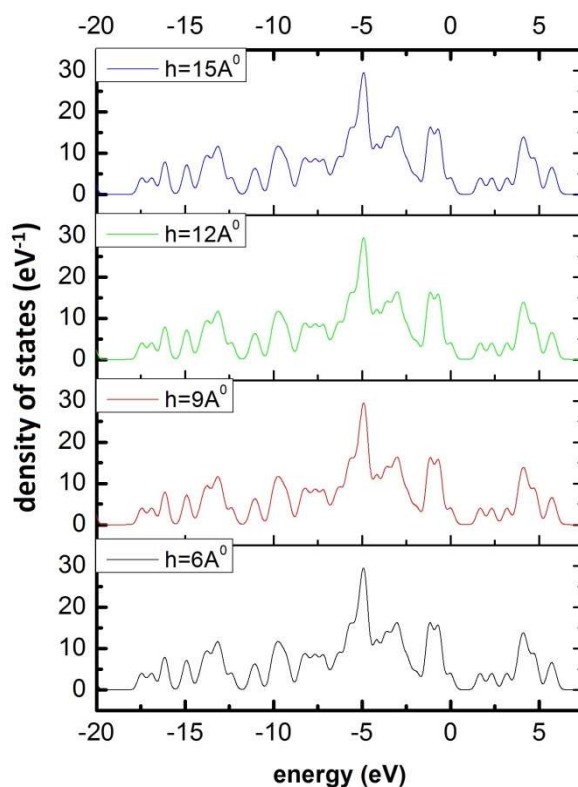
Figure 3. The electronic density in the chemotherapy band.

3.2. Effect of Impurities/Heterogeneity

When $C_{13}H_8OS–X$ is doped/modified by different atoms or functional groups: H, Br, OH, OCH_3, and OC_2H_5, the different energies of the molecule, the structure, electronic structure as a function of temperature were calculated and then plotted in Figure 4.
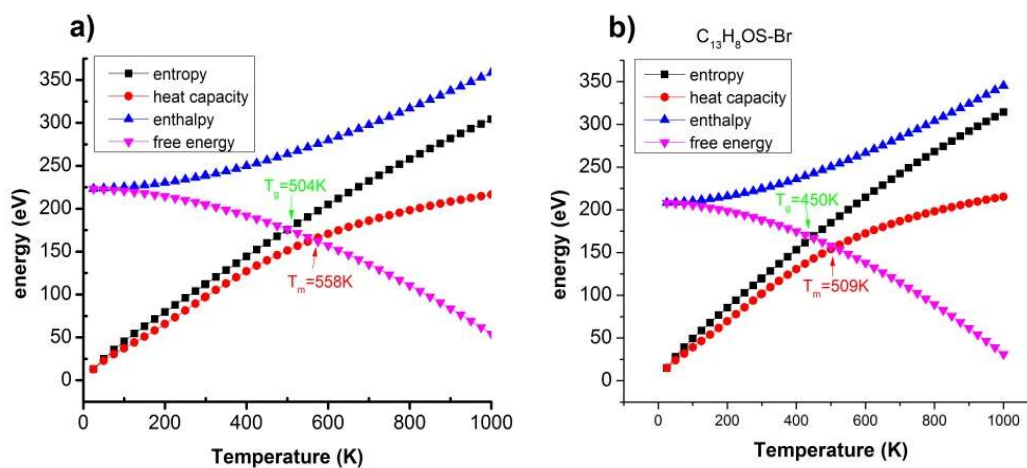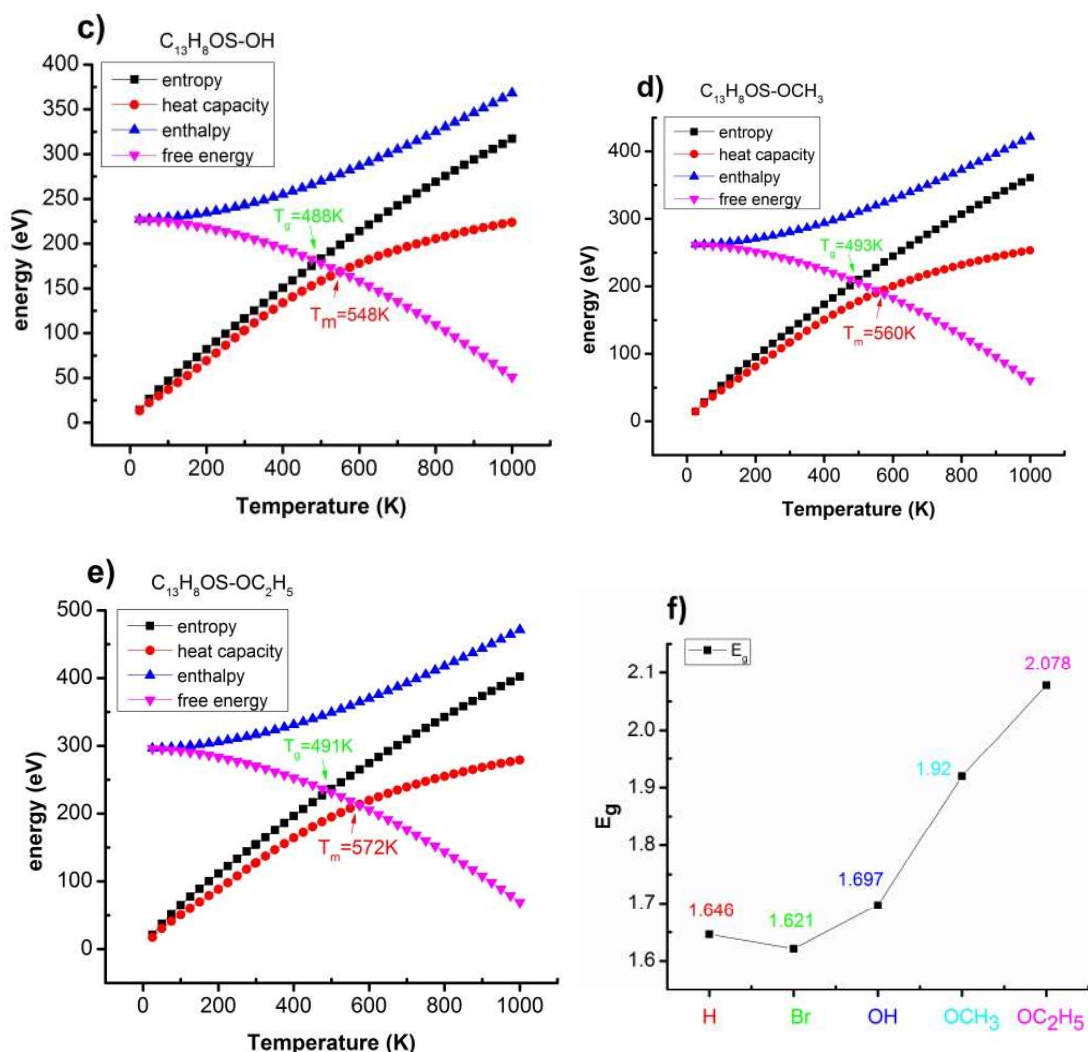

Figure 4. *Cont.*

Figure 4. The electronic structures of poly($C_{13}H_8OS–H$) (**a**), poly($C_{13}H_8OS–Br$) (**b**), poly($C_{13}H_8OS–OH$) (**c**), poly($C_{13}H_8OS–OCH_3$) (**d**), and poly($C_{13}H_8OS–OC_2H_5$) (**e**), E_g of poly with different impurities (**f**).

The results show that the material shape is poly($C_{13}H_8OS–H$) (Figure 4a), with the bandgap of E_g = 1.646 eV (Figure 4f). For poly($C_{13}H_8OS–X$) material doped/modified with X (X is H, Br, OH, OCH_3, OC_2H_5), the shapes of poly($C_{13}H_8OS–Br$), poly($C_{13}H_8OS–OH$), poly($C_{13}H_8OS–OCH_3$), and poly($C_{13}H_8OS–OC_2H_5$) have changed significantly: temperature range of phase transition of poly($C_{13}H_8OS–H$) = 504 K < T < 558 K; poly($C_{13}H_8OS–Br$) = 450 K < T < 509 K (Figure 4b); poly($C_{13}H_8OS–OH$) = 488 K < T < 548 K (Figure 5c); poly($C_{13}H_8OS–OCH_3$) = 493 K < T < 560 K (Figure 4d); poly($C_{13}H_8OS–OC_2H_5$) = 491 K < T < 572 K (Figure 4e), and the bandgap E_g decreases from E_g = 1.646 eV to E_g = 1.621 eV with poly($C_{13}H_8OS–Br$) and E_g increases with poly($C_{13}H_8OS–OH$) from E_g = 1.646 eV to E_g = 1.697 eV; E_g increased from 1.646 eV to 1.920 eV with poly($C_{13}H_8OS–OCH_3$); E_g increased from 1.646 eV to 2.078 eV with poly($C_{13}H_8OS–OCH_3$) (Figure 4f). This shows that the doping poly($C_{13}H_8OS–H$) with Br (electrophilic group) leads to a decrease of both T and E_g while doping this molecule with nucleophilic groups such as OH, OCH_3, and OC_2H_5 leads to an increment of T and E_g.

The effect of the nature of the substituents/substitution groups on the molecular shape and the electron density of the energy bands are then investigated and the obtained results are shown in Figure 5.
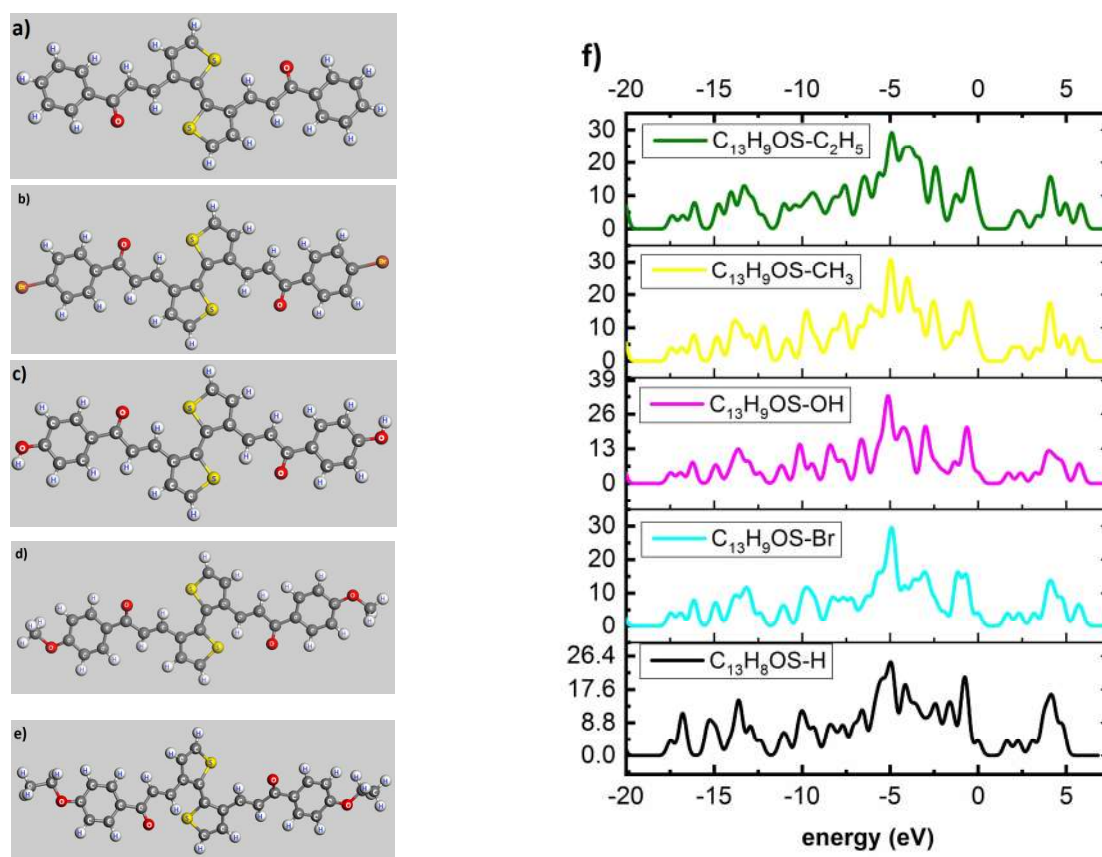
Figure 5. The structural shapes of $C_{13}H_8OS–H$ (**a**), $C_{13}H_8OS–Br$ (**b**), $C_{13}H_8OS–OH$ (**c**), $C_{13}H_8OS–OCH_3$ (**d**), $C_{13}H_8OS–OC_2H_5$ (**e**), and the electronic energies structures with poly different (**f**).

The results show that molecular shape exhibits box-shaped with a precise cell size as follows: $C_{13}H_8OS–H$: a = 24 Å, b = 133 Å and c = 6 Å; $C_{13}H_8OS–Br$: a = 26 Å, b = 133 Å, c = 6 Å; poly($C_{13}H_8OS–OH$): a = 26 Å, b = 133 Å, c = 6 Å; $C_{13}H_8OS–OCH_3$: a = 29 Å, b = 133 Å, c = 6 Å; poly($C_{13}H_8OS–OC_2H_5$): a = 32 Å, b = 133 Å, c = 6 Å. The bond angles of different poly($C_{13}H_8OS–H$) derivatives are also calculated: poly($C_{13}H_8OS–H$) with C–C–H = 120.02°; poly($C_{13}H_8OS–Br$) with C–C–Br = 119.13°; poly ($C_{13}H_8OS–OH$) with C–O–H = 109.38°; poly($C_{13}H_8OS–OCH_3$) with C–C–O = 115.62°, O–C–H = 110.56°, H–C–H = 109.66°; poly($C_{13}H_8OS–OC_2H_5$) with C–O–C = 118.28°, O–C–H = 108.79°, H–C–H = 108.79°, C–C–H = 109.22°. The electronic density of poly($C_{13}H_8OS–H$) with energy bands of E = −20, −15, −10, −5, −2.5, 0, 2.5, 5 and 7.5 eV exhibit electric densities equal to 1.728%, 8.574%, 11.993%, 24.814%, 11.434%, 3.945%, 2.022%, 4.182%, and 0%, respectively (Figure 5f). If doping the functional side groups Br, OH, CH_3, or C_2H_5 on $C_{13}H_8OS$, the electronic density will be greatly changed. For example, for energy in the range of 20 eV, the electron density increases from 1.728% to 2.55%, 4.033%, 5.667%, or 7.325%; for the energy band E = −15 eV, the electron density decreased from 8.57% to 6.02%, 5.91%, 4.83%, or 2.359%; for the E = −10 eV energy range, the electron density decreases from 11.99% to 8.01%. The obtained results show that the distance and the angle between atoms in the aromatic rings did not change significantly for $C_{13}H_8OS–H$. However, the distance between the atoms of impurities/heterogeneity varies greatly for poly($C_{13}H_8OS–H$) doped with C–H (1.09 Å—Figure 5a); poly ($C_{13}H_8OS–Br$) doped with C–Br = 1.93 Å (Figure 5b); poly($C_{13}H_8OS–OH$) doped with C–O = 1.36 Å, O–H = 0.78 Å (Figure 5c); poly($C_{13}H_8OS–OCH_3$) with C–O =1.44 Å, O–H = 1.10 Å (Figure 5d); poly($C_{13}H_8OS–OC_2H_5$) with C–O = 1.45 Å, C–C is 1.51 Å, C–H, = 1.10 Å (Figure 5e).

Besides, in the valence region, the electron density accounts for the largest proportion, reaching the extreme value in the energy band E = −5 eV. These results confirmed this is still a semiconductor material and only increasing the conductivity when doping the group Br function leads to a decrease

in the E_g bandgap, a decrease in conductivity when doping/introducing the OH, CH_3, or the C_2H_5 functional side groups leads to an increase in the E_g bandgap (Figure 5f). These results are shown in the first Brillouin region (the level of 0) corresponding to the density of electrons increased from 3.945% to 3.949%, 4.509%, 7.903% and 13.967% and this leads to an increment of the electron mobility of the $C_{13}H_8OS$ substance with Br doping but decreases with H, OH, OCH_3, and OC_2H_5 functional side groups. This confirms the influence of impurities/heterogeneity on the lattice structure and electronic structure of $C_{13}H_8OS$ material. In other words, when increasing the distance between atomic layers, the structural shape, the distance between the atoms, the total energy of the system and the bandgap are almost constant, especially the phase transition temperature and the conductivity of electrons decreases. When doping/fine-tuning with different groups and atoms such as Br, OH, OCH_3, or OC_2H_5, the distance between atoms, the total energy of the system, and the bandgap show a great change (increase the conductivity when Br is doped, reducing the conductivity when it is doped with OH, OCH_3, or OC_2H_5).

4. Conclusions

In summary, we report a successful investigation of factors affecting the structural characteristics, the transition temperature, electronic properties of Poly $C_{13}H_8OS$–X, where X are H, Br, OH, OCH_3, or OC_2H_5 by means of DFT using the GGA-PW91 package. The results showed that the interval between round one and round two: C–C: varies from 1.36 Å to 1.50 Å, C–O: 1.25 Å, C–H: 1.09 Å. The obtained results are completely consistent with the structural determination for which C–C = 1.33 Å, C–O =1.23 Å. The second round: C–C= 1.36–1.42 Å, C–S = 1.72 Å, C–H: 1.09 Å, C–H: 1.09 Å [47]. When increasing the thickness (h) of the atomic layer from h = 6 Å to h = 9, 12 and 15 Å, the transition temperature range of poly($C_{13}H_8OS$–H) shows a negligible change value from 504 K < T < 558 K to 504 K < T < 564 K and E_g increases from E_g = 1.646 eV to E_g = 1.675 eV.

The nature of the substituents (H, Br, OH, CH_3, C_2H_5) in $C_{13}H_8OS$ has a significant effect on the molecular shape and bond length. These values are successfully calculated and reported as follows: $C_{13}H_8OS$–H with C–H = 1.09 Å; $C_{13}H_8OS$–Br with C–Br = 1.93 Å; $C_{13}H_8OS$–OH with C–O = 1.36 Å, O–H = 0.78 Å; $C_{13}H_8OS$–OCH_3 with C–O = 1.44 Å, O–H = 1.10 Å; $C_{13}H_8OS$–OC_2H_5 with C–O =1.45 Å, C–C = 1.51 Å, C–H = 1.10 Å. The transition temperatures (T) can also be calculated: $C_{13}H_8OS$–H: 504 K < T < 558 K; $C_{13}H_8OS$–Br: 450 K < T < 509 K; $C_{13}H_8OS$–OH: 488 K < T < 548 K; $C_{13}H_8OS$–OCH_3: 493 K < T < 560 K; and $C_{13}H_8OS$–OC_2H_5: 491 K < T < 572 K.

When doping the $C_{13}H_8OS$ with Br the bandgap E_g decreases, while the doping/modification with H, OH, OCH_3, or OC_2H_5 leads to an increase of the electrical conductivity in $C_{13}H_8OS$. Our findings show that all derived $C_{13}H_8OS$/derivatives still display semiconductor behavior unless/except the case of Br. The precise values of the molecular structure, the chemical bonds, and bond angles provide useful information for future investigations of these new conjugated molecules, especially for potential applications in the energy field and electrical conducting materials based on conjugated polymers.

References

1. Skotheim, T.A.E. *Handbook of Conducting Polymers*; Dekker: Michigan City, IN, USA, 1986.

2. Chiang, C.K.; Park, Y.W.; Heeger, A.J.; Shirakawa, H.; Louis, E.J.; Gau, S.C.; MacDiarmid, A.G. Electrical conductivity in doped polyacetylene. *Phys. Rev. Lett.* **1977**, *39*, 1098–1101. [CrossRef]

3. Nambiar, S.; Yeow, J.T.W. Conductive polymer-based sensors for biomedical applications. *Biosens. Bioelectron.* **2011**, *26*, 1825–1832. [CrossRef]

4. Hajian, A.; Rafati, A.A.; Afraz, A.; Najafi, M. Electrosynthesis of polythiophene nanowires and their application for sensing of chlorpromazine. *J. Electrochem. Soc.* **2014**, *161*, B196–B200. [CrossRef]

5. English, J.T.; Deore, B.A.; Freund, M.S. Biogenic amine vapor detection using poly (aniline boronic acid) films. *Sens. Actuators B* **2006**, *115*, 666–671. [CrossRef]

6. Shrestha, B.K.; Ahmad, R.; Shrestha, S.; Park, C.H.; Kim, C.S. In situ synthesis of cylindrical spongy polypyrrole doped protonated graphitic carbon nitride for cholesterol sensing application. *Biosens Bioelectron.* **2017**, *94*, 686–693. [CrossRef]

7. Kumar, M.R.; Ryman, S.; Tareq, M.O.; Buchanan, D.; Freund, M.S. Chemical diversity in electrochemically deposited conducting polymer-based sensor arrays. *Sens. Actuators B* **2014**, *202*, 600–608. [CrossRef]

8. Ayenimo, J.G.; Adeloju, S.B. Amperometric detection of glucose in fruit juices with polypyrrole-based biosensor with an integrated selective layer for the exclusion of interferences. *Food Chem.* **2017**, *229*, 127–135. [CrossRef]

9. Chun, L.; Gaoquan, S. Polythiophene-based optical sensors for small molecules. *ACS Appl. Mater. Interfaces* **2013**, *5*, 4503–4510.

10. Fang, Y.; Jiang, X.; Niu, L.; Wang, S. Constructing polypyrrole/aligned carbon nanotubes composite materials as electrodes for high-performance supercapacitors. *Mater. Lett.* **2017**, *190*, 232–235. [CrossRef]

11. Zhou, X.; Chen, X.; He, T.; Bi, Q.; Sun, L.; Liu, Z. Fabrication of polypyrrole/vanadium oxide nanotube composite with enhanced electrochemical performance as a cathode in rechargeable batteries. *Appl. Surf. Sci.* **2017**, *405*, 146–151. [CrossRef]

12. Afzal, A.; Abuilaiwi, F.A.; Habib, A.; Awais, M.; Waje, S.B.; Atieh, M.A. Polypyrrole/carbon nanotube supercapacitors: Technological advances and challenges. *J. Power Sources* **2017**, *352*, 174–186. [CrossRef]

13. Ebrahimi, I.; Gashti, M.P. Chemically reduced versus photo-reduced clay-Ag-polypyrrole ternary nanocomposites: Comparing thermal, optical, electrical and electromagnetic shielding properties. *Mater. Res. Bull.* **2016**, *83*, 96–107. [CrossRef]

14. Zhao, H.; Hou, L.; Lu, Y. Electromagnetic shielding effectiveness and serviceability of the multilayer structured cuprammonium fabric/polypyrrole/copper (CF/PPy/Cu) composite. *ChemEng J.* **2016**, *297*, 170–179. [CrossRef]

15. Trung, V.Q.; van Hoan, P.; Phung, D.Q.; Duc, l.; Hang, l.T. Double corrosion protection mechanism of molybdate-doped polypyrrole/montmorillonite nanocomposites. *J. Exp. Nanosci.* **2014**, *9*, 282–292. [CrossRef]

16. Rammelt, U.; Duc, L.M.; Plieth, W. Improvement of protection performance of polypyrrole by dopant anion. *J. Appl. Electrochem.* **2005**, *35*, 1225–1230. [CrossRef]

17. Paliwoda-Porebska, G.; Rohwerder, M.; Stratmann, M.; Rammelt, U.; Duc, L.M.; Plieth, W. Release mechanism of electrodeposited polypyrrole doped with corrosion inhibitor anions. *J. Solid State Electrochem.* **2006**, *10*, 730–736. [CrossRef]

18. Grari, O.; Taouil, A.E.; Dhouibi, L.; Buron, C.; Lallemand, F. Multilayered polymer role SiO_2 composite coatings for functionalization of stainless steel: Characterization and corrosion protection behavior. *Prog. Org. Coat.* **2015**, *88*, 48–53. [CrossRef]

19. Ilangovan, G.; Pillai, K.C. Preparation and characterization of monomeric molybdate (VI) anion-doped polypyrrole electrodes. *J. Solid State Electrochem.* **1999**, *3*, 474–477.

20. Vera, R.; Schrebler, R.; Grez, P.; Romero, H. The corrosion-inhibiting effect of polypyrrole films doped with p -toluene-sulfonate, benzene-sulfonate or dodecyl-sulfate anions, as a coating on stainless steel in NaCl aqueous solutions. *Prog. Org. Coat.* **2014**, *77*, 853–858. [CrossRef]

21. Frommer, J.E.; Chance, R.R. *Encyclopedia of Polymer Science and Engineering*; Wiley: New York, NY, USA, 1986; Volume 5, p. 462.

22. Klamt, A.; Schüürmann, G. COSMO: A new approach to dielec trics screening in solvents with explicit expressions for the screening energy and its gradient. *J. Chem. Soc. Perkin Trans.* **1993**, *2*, 99–805. [CrossRef]

23. Dai, Y.; Chowdhury, S.; Blaisten-Barojas, E. Density functional theory study of the structure energetics of negatively charge doligopyrroles. *Int. J. Quantum. Chem.* **2011**, *111*, 2295–2305. [CrossRef]

24. NIST. *NIST Standard Reference Database 35*; NIST/EPA Gas-Phase Infrared Database JCAMP Format; NIST: Gaithersburg, MD, USA, 2017.

25. Ullah, H.; Shah, A.A.; Bilal, S.; Ayub, K. Doping and dedoping processes of polypyrrole: DFT study with hybrid functionals. *J. Phys. Chem. C* **2014**, *118*, 17819–17830. [CrossRef]

26. Runge, E.; Gross, E.K.U. Density-functional theory for time-dependent systems. *Phys. Rev. Lett.* **1984**, *52*, 997–1000. [CrossRef]

27. van Hoang, H.; Nguyen, T.D.; Ha, N.N. Corrosion inhibition mechanism of pyridine ion iron and its alloys using DFT. *Asian J. Chem.* **2013**, *25*, 3117–3120. [CrossRef]

28. Roth, S.; Bleier, H. Solitons in polyacetylene. *Adv. Phys.* **1987**, *36*, 385. [CrossRef]

29. Heeger, A.J.; Kivelson, S.; Schrieffer, J.R.; Su, W.P. Solitons in conducting polymers. *Rev. Mod. Phys.* **1988**, *60*, 750–781. [CrossRef]

30. Chiang, C.K.; Drury, M.A.; Gau, S.; Heeger, A.J.; Shirakawa, H.; Louis, E.J.; MacDiarmid, A.G.; Park, Y.D. Synthesis of highly conducting films of derivatives of polyacetylene. *J. Am. Chem. Soc.* **1978**, *100*, 1013–1015. [CrossRef]

31. Bhavana, A.D.; Insun, Y.; Freund, M.S. A switchable self-doped polyaniline: Interconversion between self-doped and non-self-doped forms. *J. Am. Chem. Soc.* **2004**, *126*, 52–53.

32. Winokur, W.; Moon, Y.B.; Heeger, A.J.; Barker, J.; Bott, J.C.; Shirakavm, H. X-ray scattering from sodium-doped polyacetylene: In commensurate-com mensurate and order-disorder transformations. *Phys. Rev. Lett.* **1987**, *58*, 2329. [CrossRef]

33. Moon, Y.-B.; Winokur, M.; Heeger, A.J.; Barker, J.; Bott, D.C. X-ray scattering from oriented durham polyacetylene: Structural changes after electrochemical doping. *Macromolecules* **1987**, *20*, 2457. [CrossRef]

34. Chiang, C.K.; Park, Y.W.; Heeger, A.J.; Shirakawa, H.; Louis, E.J.; MacDiarmid, A.G. Conducting polymers: Halogen doped polyacetylene. *J. Chem. Phys.* **1978**, *69*, 5098. [CrossRef]

35. Chiang, C.K.; Gau, S.C.; Fincher, C.R.; Park, Y.W.; MacDiarmid, A.G.; Heeger, A.J. Polyacetylene, (CH) x: N-Type and p-Type doping and compensation. *Appl. Phys. Lett.* **1978**, *33*, 18. [CrossRef]

36. Ma, C.-Q.; Mena-Osteritz, E.; Debaerdemaeker, T.; Wienk, M.M.; Janssen, R.A.J.; Bauerle, P. Functionalized 3D oligothiophene dendrons, and dendrimers-nove l macromolecules for organic electronics. *Angew. Chem. Int. Ed.* **2007**, *46*, 1679–1683. [CrossRef]

37. Zamoshchik, N.; Salzner, U.; Bendikov, M. Nature of Charge Carriers in Long Doped Oligothiophenes: The Effect of Counterions. *J. Phys. Chem. C* **2008**, *112*, 8408–8418. [CrossRef]

38. Zade, S.S.; Bendikov, M. Theoretical study of long oligothiophene polycations as a model for doped polythiophene. *J. Phys. Chem. C* **2007**, *111*, 10662–10672. [CrossRef]

39. Salzner, U. Does the donor-acceptor concept work for designing synthetic metals? theoretical investigation of poly (3-cyano-3′-hydroxy bithiophene). *J. Phys. Chem. B* **2002**, *106*, 9214–9220. [CrossRef]

40. Rittmeyer, S.P.; Gross, A. Structural and electronic properties of oligo- and polythiophenes modified by substituents. *Beilstein J. Nanotechnol.* **2012**, *3*, 909–919. [CrossRef]

41. Radhakrishnan, S.; Parthasar, R.; Subra mania, V.; Somanathan, N. Vibrational analysis of heterocyclic polymers: A comparative study of polythiophene, polypyrrole, and polyisothia-naphthene. *J. Chem. Phys.* **2005**, *123*, 164905. [CrossRef]

42. Radhakrishnan, S.; Ananthakrishnan, S.J.; Somanathan, N. Structure-property relationships of electroluminescent polythio-phenes: Role of nitrogen-based heterocycles as side chains. *Bull. Mater. Sci.* **2011**, *34*, 713–726. [CrossRef]

43. Patra, A.; Wijsboom, Y.H.; Leitus, G.; Bendikov, M. Tuning the band gap of low-band-gap polyselenophenes and polythiophenes: The effect of the heteroatom. *Chem. Mater.* **2011**, *23*, 896–906. [CrossRef]

44. Guay, J.; Kasai, P.; Diaz, A.; Wu, R.; Tour, J.M.; Dao, L.H. Chain-length dependence of electrochemical and electronic proper-ties of neutral and oxidized soluble.alpha. *Alpha Coupled Thiophene Oligomers Chem. Mater.* **1992**, *4*, 1097–1110.

45. Gao, J.; Niles, E.T.; Grey, J.K. J-aggregates promote efficient charge transfer doping of poly(3-hexylthiophene). *J. Phys. Chem. Lett.* **2013**, *4*, 2953–2957. [CrossRef]

46. Mena-Osteritz, E.; Zhang, F.; Gotz, G.; Reineke, P.; Bauerle, P. Optical properties of fully conjugated cyclo [n] thiophenes-an experimental and theoretical approach. *Beilstein J. Nanotechnol.* **2011**, *2*, 720–726. [CrossRef]

47. Quoc, T.V.; Thuy, D.T.T.; Thanh, T.D.; Ngoc, T.P.; Thien, V.N.; Thuy, C.N.; Meervelt, L.V. Some chalcones derived from thiophene-3-carbaldehyde: Synthesis and crystal structures. *Acta Crystallograph. Sect. E* **2019**, *75*, 957–963. [CrossRef]

48. Vu, Q.-T.; Pavlik, M.; Hebestreit, N.; Rammelt, U.; Plieth, W.; Pfleger, J. Nanocomposites based on titanium dioxide and polythiophene: Structure and Properties. *React. Funct. Polym.* **2005**, *65*, 69–77. [CrossRef]

49. Vu, Q.-T.; Pavlik, M.; Hebestreit, N.; Pfleger, J.; Rammelt, U.; Plieth, W. Electrophoretic deposition of nanocomposites formed from polythiophene and metal oxides. *Electroch. Acta* **2005**, *51*, 1117–1124. [CrossRef]

50. Trung, V.Q.; Linh, N.N.; Linh, D.K.; Pfleger, J. Synthesis and characterization of polythiophenes from hydrazone derivatives side groups. *Vietnam J. Chem.* **2016**, *54*, 730–735.

51. Trung, V.Q.; Linh, N.N.; Duong, T.T.T.; Chinh, N.T.; Linh, D.K.; Hung, H.M.; Oanh, D.T.Y. Synthesis and characterization of novel poly[4-phenyl-3-(thiophene-3-ylmethyl)-1H-1,2,4-triazole -5(4H)-thione]. *Vietnam J. Chem.* **2019**, *57*, 770–776. [CrossRef]

52. Pettifor, D.G.; Cottrell, A.H. *Electron Theory in Alloy Design*; Maney Publishing: Leeds, UK, 1992.

53. Kresse, G.; Hafner, J. Ab initio molecular dynamics for liquid metals. *Phys. Rev. B* **1993**, *47*, 558–561. [CrossRef]

54. Delley, B. An all-electron numerical method for solving the local density functional for polyatomic molecules. *J. Chem. Phys.* **1990**, *92*, 508–517. [CrossRef]

55. Bernholc, J. Computational materials science: The era of applied quantummechanics. *Phys. Today* **1999**, *52*, 30–35. [CrossRef]

56. Perdew, J.P.; Burke, K.; Ernzerhof, M. Generalizedgradient approximation made simple. *Phys. Rev. Lett.* **1996**, *77*, 3865–3868. [CrossRef] [PubMed]

57. Tsuzuki, S. Interaction energies of van der Waals and hydrogen-bonded systems calculated using density functional theory: Assessing the PW91 model. *J. Chem. Phys.* **2001**, *114*, 3949. [CrossRef]

58. Perdew, J.P.; Wang, Y. Accurate and simple analytic representation of the electron-gas correlation energy. *Phys. Rev. B* **1992**, *45*, 13244–13249. [CrossRef]

59. Monkhorst, H.J.; Pack, J.D. Special points for Brillouin-zone integrations. *Phys. Rev. B* **1976**, *13*, 5188–5192. [CrossRef]

60. Hamann, D.R.; Schlüter, M.; Chiang, C. Norm-conserving pseudopotentials. *Phys. Rev. Lett.* **1979**, *43*, 1494–1497. [CrossRef]

61. Akira, I.; Yoshiyuki, T.; Takeo, F.; Hirofumi, Y. Solid-state calculations of poly(vinylidene fluoride) using the hybrid DFT method: Spontaneous polarization of polymorphs. *Polym. J.* **2014**, *46*, 207–211.

62. Yoshiaki, Y.; Yasuteru, M.; Masayoshi, T. Proposed Mechanism for the High-Yield Polymerization of Oxyethyl Propiolates with Rh Complex Catalyst Using the Density Functional Theory Method. *Polymers* **2019**, *11*, 93.

63. Robert; Robert, G. *Parr and Weitao Yang, Density-Functional Theory of Atoms and Molecules*; Oxford University Press–Newyork Clarendon Press: New York, NY, USA, 1989.

64. Koch, W.; Holthausen, M.C. *A Chemist's Guide to Density Functional Theory*, 2nd ed.; Wiley–VCH: Hoboken, NJ, USA, 2001.

65. Søndenå, R.; Stølen, S.; Ravindran, P. Corner- versus face-sharing octahedra in AMnO3 perovskites (A = Ca, Sr, and Ba). *Phys. Rev. B* **2007**, *75*, 184105. [CrossRef]

66. Slater, J.C. A Simplification of the hartree-fock method. *Phys. Rev.* **1951**, *81*, 385–390. [CrossRef]

67. Hohenberg, P.; Kohn, W. Inhomogeneous electron gas. *Phys. Rev. B* **1964**, *136*, 864–871. [CrossRef]

68. Englisch, H.; Englisch, R. Hohenberg-Kohn theorem and non-vrepresentable densities. *Phys. A* **1983**, *121*, 253–268. [CrossRef]

69. Kohn, W.; Sham, L.J. Self-consistent equations including exchange and correlation effects. *Phys. Rev. A* **1965**, *140*, 1133–1138. [CrossRef]

70. Andersen, O.K.; Jepsen, O.; Glotzel, D. *Highlights of Condensed Matter Theory*; Elsevier: Amsterdam, The Netherlands, 1985; pp. 59–176.

71. Ruban, A.V.; Skriver, H.L. Calculated surface segregation in transition metal alloys. *Comput. Mater. Sci.* **1999**, *15*, 119–143. [CrossRef]

72. Wang, Y.; Perdew, J.P. Correlation hole of the spin-polarized electron gas, with exact small-wave-vector and high-density scaling. *Phys. Rev. B* **1991**, *44*, 298–307. [CrossRef]